Entanglement Across a Transition to Quantum Chaos

Carlos Mejía-Monasterio$^{(a)}$,* Guliano Benenti$^{(a,b)}$,† Gabriel G. Carlo$^{(a,b)}$,‡ and Giulio Casati$^{(a,b,c)}$§

$^{(a)}$*Center for Nonlinear and Complex Systems, Università degli Studi dell'Insubria, via Vallegio 11, Como 22100, Italy*
$^{(b)}$*Istituto Nazionale per la Fisica della Materia,*
Unità di Como, via Vallegio 11, Como 22100, Italy and
$^{(c)}$*Istituto Nazionale di Fisica Nucleare, Sezione di Milano, Via Celoria 16, 20133 Milano, Italy*
(Dated: May 23, 2019)

We study the relation between entanglement and quantum chaos in one- and two-dimensional spin-1/2 lattice models, which exhibit mixing of the noninteracting eigenfunctions and transition from integrability to quantum chaos. Contrary to previous studies of the behavior of entanglement across a quantum phase transition, our investigation does not refer to the ground state but to any typical many-spin quantum state. We study bipartite and pairwise entanglement measures, namely the reduced Von Neumann entropy and the concurrence, and discuss quantum entanglement sharing. Our results suggest that the behavior of the entanglement is related to the mixing of the eigenfunctions rather than to the transition to chaos.

I. INTRODUCTION

Quantum entanglement has been identified as a key ingredient in quantum communication and information processing. The content of entanglement in a particular system is considered as a resource to perform several tasks in a more efficient and more secure way than any other classical method [1, 2]. For instance, quantum teleportation protocols require to share a maximally entangled state between the sender and the receiver. In the field of quantum computation, it has been found that for the case of quantum algorithms operating on pure states, the presence of multipartite entanglement between the components constituting a quantum processor is a necessary condition to achieve an exponential speedup over classical computation [3].

On the other hand, for the operability and stability of any quantum computer, the entanglement can also play the role of the property to be minimized. The unavoidable entanglement between the quantum processor and the environment is one of the most important sources of noise and, therefore, of computational errors. The understanding and control of noise in quantum protocols is clearly needed to implement any reliable quantum computation [4, 5, 6, 7, 8, 9]. Even when a quantum processor is ideally isolated from the environment, *i.e.*, in situations where the decoherence time of the processor is very large as compared to the computational time scales, the operability of the quantum computer is not yet guaranteed [10]. Indeed, also the presence of device imperfections hinders the implementation of any quantum computation. A quantum computer is a quantum many-body system. The interaction among the qubits composing the quantum registers of the computer is needed to produce the necessary amount of entanglement. Moreover, device imperfections like small inaccuracies in the coupling constants induce errors. Above a certain imperfection strength threshold (*chaos border*), quantum chaos sets in [10, 11, 12, 13]. In such a regime, exponentially many states of the computational basis are mixed after a chaotic time scale. This sets an upper time limit to the stability of a generic superposition of states coded in the quantum computer wave function. A necessary requirement for quantum computer operability and fault tolerant computation schemes is the possibility to operate many quantum gates inside the chaotic time scale.

For the case of many-body systems, the transition to chaos has been studied for fermions and bosons (see e.g. [14] and references therein), and particularly for lattice spin systems [15]. In fermionic systems with two-body interactions it has been found that, if the interaction strength exceeds some critical value, fast transition to chaos occurs in the Hilbert space of many-particle states [16]. This is commonly studied in terms of the transition between the different spectral statistics of integrable and chaotic systems. For systems with a finite size, this transition is smooth and only a crossover border where the transition occurs can be identified. The question whether this smooth transition becomes sharp in the thermodynamical limit is still under debate. However, in some cases a sharp transition to chaos is found, *e.g.*, in the three-dimensional Anderson model [17].

In a different context, the behavior of quantum entanglement across a quantum phase transition has recently attracted much attention. Quantum phase transitions (QPT) consist in a qualitative change in the ground state of the system as some control parameter is varied [18]. Unlike classical phase transitions, QPT occur at zero temperature and the fluctuations developed at the critical point are fully quantum. These fluctuations dominate the behavior of the system near the critical point, where

*Electronic address: carlos.mejia@uninsubria.it; URL: http://scienze-como.uninsubria.it/complexcomo
†Electronic address: giuliano.benenti@uninsubria.it
‡Electronic address: gabriel.carlo@uninsubria.it
§Electronic address: giulio.casati@uninsubria.it

correlations are long-range in character. It has been recently pointed out that the genuine quantum character of quantum phase transitions is due to entanglement [19]. It has also been argued that the ground state of the system is strongly entangled at the critical point [19, 20]. Therefore, the behavior of entanglement across QPT is particularly interesting for quantum computation and communication, where a maximization of the content of entanglement is desirable. The study of the relation between QPT and entanglement has been focused on the possible universal behavior of the entanglement content at the transition [21, 22, 23, 24, 25, 26, 27, 28, 29]. The dependence of entanglement on disorder and its interplay with chaos has also been studied [30, 31, 32]. Moreover, the evolution of entanglement in quantum algorithms simulating quantum chaos has been recently investigated [33, 34, 35, 36].

The aim of this paper is to characterize the behavior of quantum entanglement in non-integrable systems when a transition to quantum chaos occurs. We are interested in understanding how the entanglement content behaves in transitions from integrability to chaos. We would like to stress that, differently from previously considered models [21, 22, 23, 24, 25, 26, 27, 28, 29], the transition to chaos is not a property of the ground state but takes place for any typical many-body state. We numerically study two lattice models of interacting many spins that show a transition to chaos. They have previously been studied as models of the quantum computer hardware [10, 11, 12, 13]. In both models, the transition to chaos is driven by the strength of the interaction among the spins. We will consider bipartite and pairwise entanglement measures and focus on the relation between the entanglement and the onset of chaos. Even though, due to numerical limitations, we are unable to discuss any possible finite-size scaling for the behavior of the entanglement at the chaos border we will find that the behavior of pairwise entanglement is similar to that found in a QPT. We will also show that the behavior of entanglement is related to the mixing of noninteracting eigenfunctions rather than to the transition to chaos.

This paper is organized as follows. In Sec. II we review the measures of entanglement that we will use. The measures that signal the onset of quantum chaos are reviewed in Sec. III. In Sec. IV we define the spin lattice models investigated in this paper and discuss numerical results on their entanglement content and their transition to chaos. In Sec. V we present our final remarks.

II. MEASURES OF ENTANGLEMENT

A pure state $|\psi\rangle$ is said to be separable if for a given partition of its Hilbert space $\mathcal{H} = \mathcal{H}_A \otimes \mathcal{H}_B$ it can be written as $|\psi\rangle = |a\rangle \otimes |b\rangle$. Here $|a\rangle$ and $|b\rangle$ are vectors residing in the Hilbert subspaces $\mathcal{H}_A$ and $\mathcal{H}_B$, respectively. The pure state $|\psi\rangle$ is entangled if it is not separable.

A. Von Neumann entropy

Pure bipartite entanglement is measured in terms of the reduced Von Neumann entropy S. For a pure state the reduction of its density matrix $\rho = |\psi\rangle\langle\psi|$ is obtained through partial trace of one the two partitions as $\rho_A = \mathrm{tr}_B \rho$ or, equivalently, $\rho_B = \mathrm{tr}_A \rho$. Then, S is defined as

$$S = S_A = S_B = -\mathrm{tr}_B(\rho_B \log \rho_B) . \tag{1}$$

The Von Neumann entropy provides an unambiguous measure of entanglement for a bipartite system in an overall pure state. For a separable state $S = 0$ while for a maximally entangled state $S = \log \mathcal{N}$, where $\mathcal{N} = \min(\mathcal{N}_A, \mathcal{N}_B)$, with $\mathcal{N}_A = \dim(\mathcal{H}_A)$ and $\mathcal{N}_B = \dim(\mathcal{H}_B)$. In what follows we will take the logarithm in Eq. (1) base 2. Thus, for a many-qubit system, the maximum value that the Von Neumann entropy can take is equal to the number of qubits that have not been traced out to obtain the reduced density matrix.

B. Concurrence and entanglement of formation

For the case of mixed states, the Von Neumann entropy is no longer a good measure of entanglement. If we consider a bipartite system on an overall mixed state, then each subsystem can have non-zero entropy even if there is not any entanglement [37]. In order to measure the bipartite entanglement of a mixed state we shall consider the so-called entanglement of formation E_F [38]. Starting from a mixed state with density matrix $\rho = \sum_i p_i |\psi_i\rangle\langle\psi_i|$, $E_F(\rho)$ is defined as the average entanglement of the pure states of a given decomposition of the mixed state ρ, minimized over all its possible decompositions:

$$E_F(\rho) = \min_{\{p_i, \psi_i\}} \sum_i p_i E(|\psi_i\rangle) . \tag{2}$$

Here $E(|\psi_i\rangle)$ is the amount of entanglement of the pure state $|\psi_i\rangle$, measured, as discussed in the previous subsection, by the reduced Von Neumann entropy.

Eq. (2) is operationally difficult to handle, since it involves an extremal condition. However, for the case of two-qubit systems, E_F can be expressed in terms of a much more amenable quantity, the so-called concurrence C [39]. We have

$$E_F(\rho) = h\left(\frac{1}{2}\left[1 + \sqrt{1 - C(\rho)^2}\right]\right) , \tag{3}$$

where $h(x)$ is the so-called binary entropy function defined by

$$h(x) = -x \log_2 x - (1-x) \log_2(1-x) . \tag{4}$$

The concurrence $C(\rho)$ of the two-qubit state ρ is defined as

$$C(\rho) = \max\{0, c_\lambda\} , \tag{5}$$

where $c_\lambda = \lambda_1 - \lambda_2 - \lambda_3 - \lambda_4$, the $\{\lambda_i\}$ being the square roots of the eigenvalues of the matrix $\rho(\sigma_y \otimes \sigma_y)\rho^*(\sigma_y \otimes \sigma_y)$, in decreasing order, and σ_y a Pauli matrix. Note that in this definition the complex conjugation is taken in the computational basis $\{|00\rangle, |01\rangle, |10\rangle, |11\rangle\}$, where $|0\rangle$ and $|1\rangle$ are the eigenstates of σ_z. From Eq. (3) we see that E_F depends monotonously on the concurrence, which takes values between 0 for separable states and 1 for maximally entangled states. Moreover, it is easy to see that c_λ take values in $[-1/2, 1]$. Thus, it is clear from Eq. (5) that a state is separable if $c_\lambda \leq 0$ and entangled otherwise.

Other measures for pairwise entanglement exist. Among them we mention the entanglement of distillation [40], the negativity [41] and the relative entropy [42]. All these quantities are related in one way or another to the concurrence. Therefore, we have chosen to present our results in terms of the concurrence. Nevertheless, we mention that we have also measured the negativity and found that it essentially gives the same results as the concurrence.

Finally, for the case of multipartite entanglement the problem is much more subtle. Different measures of multipartite entanglement have been proposed, giving different results, even qualitatively [43]. We have computed the multipartite entanglement on pure states following [44]. We have found that this multipartite measure shows equivalent qualitative behavior than the averaged Von Neumann entropy. Not surprisingly, it has been shown that this measure corresponds to an average of the linear entropy [45]. Given the state of affairs, we will limit ourselves to discuss the existence of multipartite entanglement in terms of the qualitative information that can be extracted by comparing the averaged Von Neumann entropy for subsystems of different sizes.

III. TRANSITION TO QUANTUM CHAOS

Random Matrix Theory was introduced to describe the spectral properties of complex heavy nuclei. The key idea behind RMT is to replace the full physical description of the Hamiltonian by a suitable statistical representative of its symmetry group [46]. The statistical spectral fluctuations of almost any complex Hamiltonian were found to be described by a few classes of random matrix ensembles. This approach turned out to be very successful. The RMT analysis has been applied to many fields of physics such as nuclei, atoms, molecules, quantum dots, quantum billiards and many-body systems among others [14, 15, 47, 48, 49, 50]. In the early 1980's it was conjectured that the quantum versions of integrable and chaotic classical systems were described by different classes of random ensembles [51, 52]. Since then, RMT has been successfully applied to describe the emergence of quantum signatures of chaos.

The global manifestation of the onset of chaos in quantum systems consists of a very complex structure of the

quantum states as well as of spectral fluctuations that are statistically described by Random Matrix Theory (RMT) [46]. Let us focus on many-particle systems with two-body interaction as this is the nature of the model systems that we study in this paper. For this kind of systems it has been found that, under very general conditions, if the interaction strength exceeds some critical value, fast transition to chaos occurs in the Hilbert space of many-particle states.

To be more precise let us consider a generic perturbed quantum many-body system. The Hamiltonian can be split into two parts:

$$H = H_0 + V \ , \tag{6}$$

where H_0 corresponds to the unperturbed original Hamiltonian and the perturbation V to an interacting term. The unperturbed Hamiltonian H_0 is assumed integrable. In other words, when $V = 0$ the existence of as many integrals of motion as degrees of freedom is assumed. We will take the unperturbed eigenstates of the non-interacting Hamiltonian H_0 to span the many-particle Hilbert space. In this basis, when the interaction is turned on, the eigenstates start to mix. The mixing can be described, for small interaction strengths, by perturbation theory. However, perturbation theory breaks down and quantum chaos sets in when the typical interaction matrix element between directly coupled states becomes of the order of their energy separation [16] (we say that two many-body states $|\psi_1\rangle$ and $|\psi_2\rangle$ are directly connected if $\langle\psi_1|V|\psi_2\rangle \neq 0$). The transition to chaos reflects in the statistical properties of the spectrum.

A. Nearest neighbor level spacing distribution

The nearest neighbor level spacing distribution $P(s)$ is the probability density to find two adjacent levels at a distance s.

For an integrable system the distribution $P(s)$ has typically a Poisson distribution

$$P_{\mathrm{P}}(s) = \exp(-s) \ . \tag{7}$$

In contrast, in the quantum chaos regime, for Hamiltonians obeying time-reversal invariance, the nearest neighbor spacing distribution corresponds to the Gaussian Orthogonal Ensemble of random matrices (GOE). This distribution is well-approximated by the Wigner surmise, which reads

$$P_{\mathrm{WD}}(s) = \frac{\pi s}{2} \exp\left(-\frac{\pi s^2}{4}\right) \ . \tag{8}$$

Note that the GOE distribution exhibits the so-called "level repulsion", *i.e.*, the probability to find close energy levels is very small. This is in contrast to what is observed for integrable systems which exhibit level clustering. An example of Poisson and Wigner distributions is provided in Fig. 4.

In Eqs. (7) and (8) the level spacing s is given in units of the mean level spacing Δ, which we have set equal to 1.

The transition to quantum chaos may be detected by the change of the nearest neighbor spacing distribution $P(s)$ from Poisson to GOE. In order to obtain a more quantitative measure of this transition, it is useful to compute the parameter

$$\gamma = \frac{\int_0^{s_0} [P(s) - P_{\text{WD}}(s)] \, \mathrm{d}s}{\int_0^{s_0} [P_{\text{P}}(s) - P_{\text{WD}}(s)] \, \mathrm{d}s} \, , \qquad (9)$$

where $s_0 \approx 0.4729$ corresponds to the lowest s-value at which the Poisson [Eq. (7)] and Wigner [Eq. (8)] curves cross. This parameter takes values 1 and 0 for the Poisson and Wigner distributions, respectively.

The distribution $P(s)$ describes the behavior of the fluctuations at energy scales of the order of Δ. Therefore, $P(s)$ is a short range correlation. The effects of the onset of quantum chaos are also seen in higher moments of the distribution of energy levels. However, we will limit ourselves to the analysis of $P(s)$ as a spectral signature of the transition to quantum chaos.

B. Inverse participation ratio

The effects of the onset of chaos can also be observed in the eigenfunctions. The transition reflects in the degree of mixing of the eigenfunctions of the system. However, the eigenfunction-based measures are more subtle. This is because the mixing of eigenfunctions is a basis-dependent quantity. Clearly, if the eigenfunctions are expanded in their own basis, they are not mixed at all, independently of the fact that the distribution $P(s)$ is Poisson or GOE. Nevertheless, for Hamiltonians of the type (6) the increase of typical eigenfunctions' mixing with perturbation is naturally obtained in the basis $\{|i\rangle\}$ of the unperturbed Hamiltonian H_0 [53].

In the basis $\{|i\rangle\}$ the mixing (or, equivalently, the *delocalization*) of a given eigenstate $|\psi\rangle$ is customarily measured in terms of the number of components $\langle i|\psi\rangle$ which are significantly different from zero: A useful quantity to measure the degree of delocalization of a given eigenstate is the so-called Inverse Participation Ratio (IPR), defined as

$$\xi = \frac{1}{\sum_i |\langle i|\psi\rangle|^4} \, . \qquad (10)$$

If the state $|\psi\rangle$ is maximally localized, all its components are zero but one, with value $|\langle i|\psi\rangle|^2 = 1$ due to normalization. Therefore, in the localized regime $\xi \approx 1$, while ξ increases with increasing mixing. In the thermodynamic limit, ξ is unbounded. However, in the case of finite size systems $\xi \leq N$, where N is the dimension of the Hilbert space. For the GOE case, the IPR is equal to $\xi = N/3$, due to the statistical properties of the chaotic states.

Even though, in general, the transition from localized to delocalized eigenfunctions occurs in parallel with the transition from Poissonian to Wigner spectra, this is not always the case. As we will study in the following sections, for particular model systems the spectra can be uncorrelated even in situations in which the eigenfunctions are delocalized. It is common to term this situation as *weak chaos*.

C. Chaos and entanglement

It is worthwhile to discuss what are the expectations for the entanglement content in the nearly integrable and fully chaotic situations. Let us consider a many-particle system with a Hamiltonian as in Eq. (6) and let $\mathcal{N}$ denote the dimension of its Hilbert space. In a given basis $\{|n\rangle\}$ the density matrix for an eigenstate of the system, $|\psi\rangle = \sum_n c_n |n\rangle$, writes as follows:

$$\rho_{nm} = \langle n|\psi\rangle\langle\psi|m\rangle = c_n c_m^* \, , \qquad (11)$$

where $c_n = \langle n|\psi\rangle$ are the components of the eigenstate in the $\{|n\rangle\}$ basis. As discussed in the previous subsection, the nearly integrable case corresponds to a situation of weak interaction. This implies that in the basis of the unperturbed Hamiltonian H_0 the eigenfunctions are localized, i.e., $c_n \approx \delta_{n,n^\star}$ for some $n^\star \in [1, \mathcal{N}]$. Therefore, the density matrix will have all entries nearly equal to zero, except for the diagonal matrix element $\rho_{n^\star n^\star} = |c_{n^\star}|^2 \approx 1$. At the other extreme of strong interaction, in which quantum chaos has set in, the eigenfunctions are fully extended. In this situation the eigenstates can be considered as random states with uniformly distributed components with amplitudes $c_n \approx 1/\sqrt{\mathcal{N}}$ and random phases. In this case, the density matrix can be written as

$$\rho \approx \text{diag}\left(1/\mathcal{N}, 1/\mathcal{N}, \ldots, 1/\mathcal{N}\right) + \Omega \, , \qquad (12)$$

where Ω is a $\mathcal{N} \times \mathcal{N}$ zero diagonal matrix with random complex matrix elements of amplitude $\approx 1/\mathcal{N}$.

Suppose now that we partition the Hilbert space of the system into two parts with dimensions $\mathcal{N}_A$ and $\mathcal{N}_B$, where $\mathcal{N}_A \mathcal{N}_B = \mathcal{N}$. The reduced density matrix ρ_A is defined as follows:

$$\rho_A = \text{Tr}_B \rho = \sum_{n_B} c_{n_A n_B} c_{n'_A n_B}^\star |n_A\rangle\langle n'_A| \, , \qquad (13)$$

where $|n\rangle = |n_A n_B\rangle$. Therefore, in the integrable case the reduced density matrix ρ_A is a $\mathcal{N}_A \times \mathcal{N}_A$ matrix given by

$$\rho_A \approx \text{diag}\left(0, 0, \ldots, 0, 1, 0, \ldots, 0\right) \, . \qquad (14)$$

In contrast, in the chaotic case

$$\rho_A \approx \text{diag}\left(1/\mathcal{N}_A, 1/\mathcal{N}_A, \ldots, 1/\mathcal{N}_A\right) + \Omega_A \, , \qquad (15)$$

where Ω_A is a zero diagonal matrix with matrix elements of $\mathcal{O}\left(\sqrt{\mathcal{N}_B}/\mathcal{N}\right)$ (sum of $\mathcal{N}_B$ terms of order $1/\mathcal{N}$ with random phases).

With Eqs. (14) and (15) in hand, it is easy to calculate the values for the reduced Von Neumann entropy and the concurrence. We have

$$S_A \approx \begin{cases} 0 & \text{for integrable regime} \\ \log(\mathcal{N}_A) & \text{for chaotic regime} \end{cases} . \quad (16)$$

A better estimate of S_A is obtained by considering the ensemble of random states according to the Haar measure: $S_A \approx \log(\mathcal{N}_A) - \mathcal{N}_A/(2\mathcal{N}_B \log_e 2)$ [54].

For the case of concurrence the dimension $\mathcal{N}_A = 4$. If in Eqs. (14)-(15) we neglect the matrix Ω_A we obtain

$$c_\lambda \approx \begin{cases} 0 & \text{for integrable regime} \\ -1/2 & \text{for chaotic regime} \end{cases} . \quad (17)$$

Thus, in both integrable and chaotic extremes, we obtain from Eq. (5) that the concurrence is zero. Nevertheless, as we have discussed above, this zero concurrence is due to very different physical reasons.

IV. CHAOS AND ENTANGLEMENT IN SPIN CHAINS

In this Section, we discuss bipartite and pairwise entanglement measures in two quantum lattice spin models in which a transition to chaos has been found and characterized. Both models have been proposed as suitable model for quantum computers. For the sake of completeness in this section we review the known properties of these models, in particular the onset of quantum chaos. In parallel, we present new results concerning the behavior of quantum entanglement.

A. Two-dimensional spin lattice

The first model we consider consists of L spin-1/2 particles (qubits) placed on a two-dimensional square lattice in the presence of an external static magnetic field directed along z. Nearest-neighbor spins interact via Ising coupling with random strength. The Hamiltonian of the system is

$$H = \sum_i \Gamma_i \sigma_i^z + \sum_{i<j} J_{i,j} \sigma_i^x \sigma_j^x . \quad (18)$$

The operators σ_i are the standard Pauli matrices acting on the i-th qubit. The second sum in the Hamiltonian runs over nearest-neighbor spins and periodic boundary conditions are considered. Γ_i corresponds to the energy separation between the states of the qubit i. $J_{i,j}$ is the interaction strength between the qubits i and j. The parameters Γ_i and $J_{i,j}$ are randomly and uniformly distributed in the intervals $[\Delta_0 - \delta/2, \Delta_0 + \delta/2]$ and $[-J, J]$, respectively. This Hamiltonian was proposed as a model of isolated quantum computer with hardware imperfections [10].
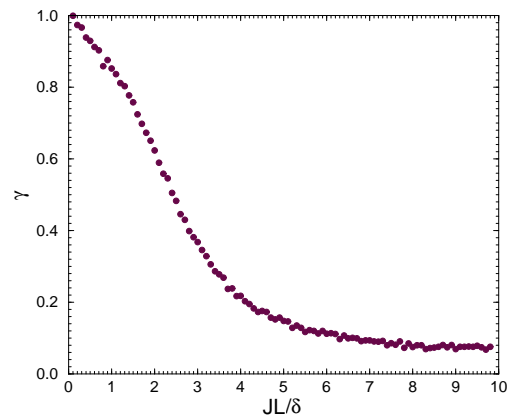

FIG. 1: Level statistics parameter γ as a function of the coupling parameter J (in units of $\delta/L \propto J_{\text{cr}}$), for the model of Eq. (18) for a 3×3 lattice, calculated from the energy levels in the central negative band of the spectrum. The other parameters are $\Delta_0 = 1$ and $\delta = 0.09$.

Here we focus on the case $\delta, J \ll \Delta_0$, which corresponds to the situation where fluctuations induced by lattice imperfections are relatively weak. In this case, the unperturbed energy spectrum ($J_{i,j} = 0$) of Hamiltonian (18) is composed by $L+1$ well separated bands, with inter-band spacing $2\Delta_0$. Each band corresponds to states with a given number of spins "up" and spins "down". The highest density of states is obtained for the central energy band and therefore we expect that quantum chaos shows up first there. When interaction is turned on, a transition to chaos takes place. The critical border J_{cr} for this transition was obtained in [10]: $J_{\text{cr}} \propto \delta/L$. This border was corroborated in [12], where the emergence of Fermi-Dirac thermalization in the chaotic regime was studied. A careful and detailed analysis of the transition to chaos for this model and its dependence on the size of the lattice has been taken in [10, 12]. Here, we consider a square 3×3 lattice. We note that for lattices composed of an odd number of qubits there is not a central energy band but instead, two central bands, one negative and one positive. In what follows, we will consider the central negative band alone.

We have numerically diagonalized Hamiltonian (18) for different values of the interaction strength. To study the transition to chaos we have obtained the spectral statistics in terms of the nearest neighbor spacing distribution $P(s)$ as well as the structure of the eigenfunctions in terms of the inverse participation ratio ξ. We have restricted our calculations to the energies and eigenstates encountered in the central negative band. For weak interactions the energy domain of this band is clearly visible and we keep the same domain even for stronger interaction where the band structure disappears.

In Fig. 1 the parameter γ as a function of the interaction strength is shown for $\Delta_0 = 1$ and $\delta = 0.09$. When the strength of the interaction J increases the $P(s)$ distri-
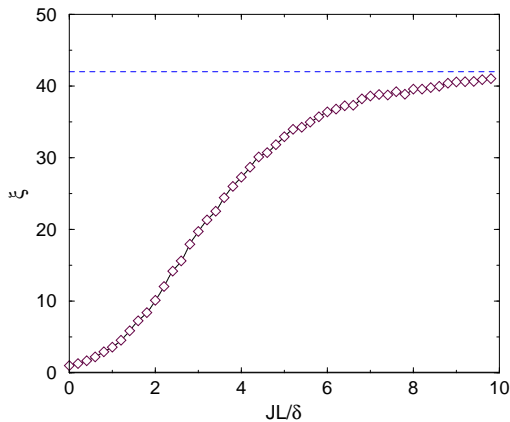
FIG. 2: Inverse participation ratio ξ as a function of JL/δ for the model of Eq. (18) for a 3×3 lattice, with parameter values as in Fig. 1. The IPR was obtained from the central eigenfunction of the central negative band of the spectrum averaged over 2000 random realizations of δ_i and $J_{i,j}$. The dashed line corresponds to $N_b/3$.
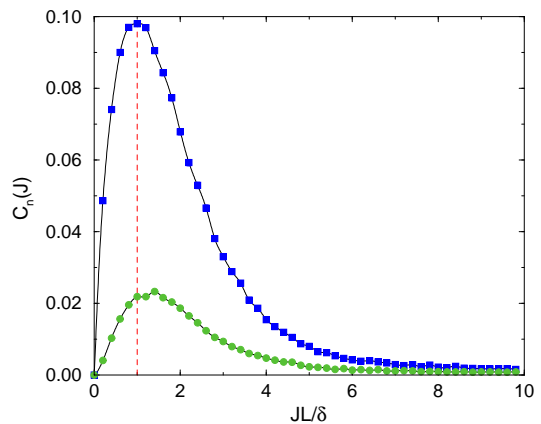

FIG. 3: Concurrence C_n as a function of the coupling parameter JL/δ for the model of Eq. (18) for a 3×3 lattice, with parameter values as in Fig. 1. C_n was obtained from the central eigenfunction of the central negative band of the spectrum and averaged over all possible pairs of: a) nearest neighbors qubits ($n = 1$) and b) next to nearest neighbors qubits ($n = 2$). The vertical dashed line marks the value $JL/\delta = 1$.

bution smoothly changes from Poisson ($\gamma = 1$) towards GOE ($\gamma = 0$). Thus, increasing the interaction among the qubits a transition to quantum chaos occurs. In Fig. 1 we observe that the crossover from integrability to chaos takes place in the interval between $JL/\delta \approx 1$ and $JL/\delta \approx 5$.

At the same time, the eigenfunctions start to mix. For weak interactions the eigenfunctions are strongly localized: The number of components in the basis of the unperturbed Hamiltonian is of the order of one. At strong interactions ($JL/\delta \gg 1$) the eigenfunctions are extended, having a large number of non negligible components. This mixing of the eigenfunctions is shown in Fig. 2 in terms of the IPR for the same parameter values as in Fig. 1. In Fig. 2 we see that the IPR smoothly changes from 1 (localized regime) to $N_b/3$ (chaotic regime), where N_b corresponds to the number of eigenfunctions with energies in the central negative band. As we have said, the factor $1/3$ arises due to the symmetries of the chaotic Hamiltonians which are described by the GOE.

We now turn our attention to the entanglement measures. We have calculated the concurrence between nearest (C_1) and next to nearest (C_2) neighbor qubits. For this purpose we have drawn 2000 random realizations of δ_i and $J_{i,j}$ and diagonalized Hamiltonian (18). Using for each realization only the central eigenfunction of the central negative band we have calculated the mean concurrence averaged over all possible nearest neighbor pairs of qubits. In Fig. 3 we show C_1 (squares) and C_2 (circles), averaged over all the random realizations as a function of the strength of the interaction. In the basis of the unperturbed Hamiltonian the concurrence is strictly zero. For very weak interactions ($JL/\delta \ll 1$), the concurrence remains small. At the other extreme, when the interaction is very strong ($JL/\delta \gg 1$) and quan-

tum chaos has set in, the concurrence is also small, as expected. Quite interestingly, the maximum of the C_1 concurrence is for $JL/\delta \approx 1$, that is, in the region in which the crossover from integrability to quantum chaos takes place. In Fig. 3 we can also compare the behavior of C_1 with that of C_2. The concurrence of next to nearest neighbor qubits is noticeable smaller than that of nearest neighbor qubits. This is not surprising as the Ising interaction in Eq. (18) couples only nearest neighbor qubits. Therefore, one should expect that quantum correlations among qubits are stronger for qubits that are close than for those farther away. However, we find that C_2 is not negligible everywhere over the domain of J investigated, except for the integrable and chaotic extremes, where also C_1 goes to zero. Similarly to C_1, the concurrence C_2 has its maximum value for $JL/\delta \approx 1$. It is worthwhile mentioning that this behavior is qualitatively similar to that found for the concurrence across a quantum transition to chaos.

To investigate more deeply the relation between transition to chaos and entanglement it would be desirable to see how the concurrence behaves for larger lattice sizes. Unfortunately, this is not easy to realize for the model of Eq. (18). In view of these limitations, in the next section we study a one-dimensional lattice model for which a comparison of the behavior of entanglement for different lattice sizes is possible.

B. One-dimensional spin chain

In this section we discuss the behavior of bipartite and pairwise entanglement in a family of models describing

one-dimensional spin 1/2 chains. These models will allow us to characterize the behavior of the entanglement across the transition to chaos in a deeper fashion than for the previous two-dimensional model. We shall find that, similarly to the two-dimensional model, the concurrence exhibits a maximum close to the border for the transition to chaos. Moreover, due to the lower dimensionality, we will be able to analyze the dependence of the concurrence on: the distance in the lattice between the partners, the range of the interaction and the size of the chain. Furthermore, for one member of this family of models the chaos border does not coincide with the delocalization border. This will give us the possibility to compare the behavior of the concurrence in regimes of weak and hard chaos.

1. Definition of the model.

We consider a system consisting on a linear chain of L 1/2 interacting spins, subjected to a static transverse magnetic field (along z) and to a circularly polarized magnetic field rotating in the (x, y) plane with frequency ν, $\vec{B}(t) = (B^\perp \cos(\nu t + \varphi), -B^\perp \sin(\nu t + \varphi), B^z)$ [13]. In the coordinate system, which rotates around the z axis with frequency ν, the Hamiltonian of this system can be written as

$$
\begin{aligned}
H = &-\tfrac{1}{2} \sum_{k=1}^{L} \{\delta_k \sigma_k^z + \Omega(\cos\varphi \ \sigma_k^x - \sin\varphi \ \sigma_k^y)\} \\
&+ \tfrac{1}{2} \sum_{k=1}^{L-1} J_{k,k+1} \sigma_k^z \sigma_{k+1}^z,
\end{aligned}
\tag{19}
$$

$\delta_k = \omega_k - \nu$ where ω_k is the frequency of the precession of the k-th spin in the B^z field. Ω stands for the Rabi frequency corresponding to the rotating field and $J_{k,k+1}$ denotes the strength of the Ising interaction between the spins k and $k+1$. The operators σ_k are the standard Pauli operators acting on the k-th spin. In the following, we will take for simplicity $\varphi = \pi/2$ and consider that the static field B^z has a constant gradient a along the chain such that $\delta_k = ak$. Thus, the Hamiltonian takes the form

$$
H = \frac{1}{2} \sum_{k=1}^{L} (-\delta_k \sigma_k^z + \Omega \sigma_k^y) - \frac{1}{2} \sum_{k=1}^{L-1} J_{k,k+1} \sigma_k^z \sigma_{k+1}^z \ , \tag{20}
$$

We assume that for all k the inequality $\Omega \gg \delta_k$ holds. Open boundary conditions are taken. In [13], this model was proposed as a possible candidate for experimental realization of quantum computation. The gradient of magnetic field provides a labeling of qubits in terms of their Larmor frequencies. Thus, it allows for a way to address each qubit separately.

It is worthwhile mentioning that, besides the different dimensionality, there is a more striking difference between this and the previous model: The existence of a constant gradient in the magnetic field gives rise to a L-independent threshold for the onset of (weak) chaos. In
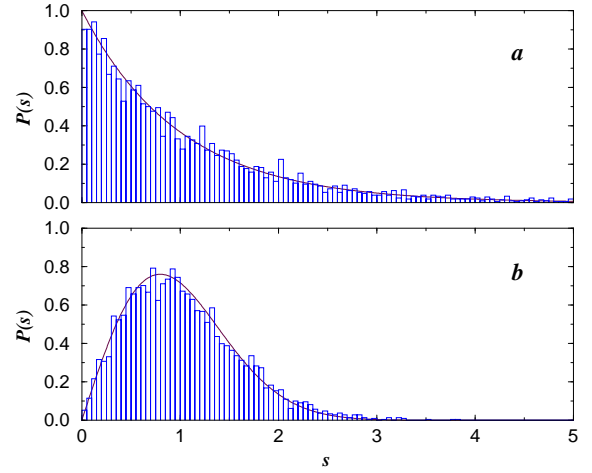

FIG. 4: Nearest neighbor level spacing distribution $P(s)$ for the AA model ($l_c = L - 1$) of Eq. (25) for a chain of 12 qubits and: a) $J/J_{cr} = 0.35$ and b) $J/J_{cr} = 15$, calculated from the energy levels in the central band of the spectrum and averaged over 10 random realizations. The solid lines correspond to the Poisson (a) and Wigner surmise (b) theoretical distributions.

[13] the transition to quantum chaos and its implications to quantum computation were explored. Here we want to discuss the behavior of entanglement in this model.

In order to apply the approach discussed in section III it is convenient to represent Hamiltonian (20) in the basis in which it is diagonal for non-interacting spins. In this so-called effective field representation, the one-body unperturbed Hamiltonian H_0 takes the form

$$
H_0 = \frac{1}{2} \sum_{k=1}^{L} \sqrt{\delta_k^2 + \Omega^2} \ \sigma_k^z \tag{21}
$$

and the interaction Hamiltonian V can be written as $V = V_{\text{diag}} + V_{\text{band}} + V_{\text{off}}$, where

$$
V_{\text{diag}} = -\frac{1}{2} \sum_{k=1}^{L-1} J_{k,k+1} b_k b_{k+1} \sigma_k^z \sigma_{k+1}^z,
$$

$$
V_{\text{band}} = -\frac{1}{2} \sum_{k=1}^{L-1} J_{k,k+1} a_k a_{k+1} \sigma_k^y \sigma_{k+1}^y, \tag{22}
$$

$$
V_{\text{off}} = \frac{1}{2} \sum_{k=1}^{L-1} J_{k,k+1} \left(a_k b_{k+1} \sigma_k^y \sigma_{k+1}^z + a_{k+1} b_k \sigma_k^z \sigma_{k+1}^y \right),
$$

with

$$
a_k = \frac{\Omega}{\sqrt{\delta_k^2 + \Omega^2}} \quad , \quad b_k = \frac{-\delta_k}{\sqrt{\delta_k^2 + \Omega^2}} \ . \tag{23}
$$

As before, the quantities $J_{k,k+1}$ stand for the Ising interactions between nearest neighbor spins. In what follows, we will consider the interactions to be completely random, i.e. $J_{k,k+1} = J\xi$, where ξ is a random number
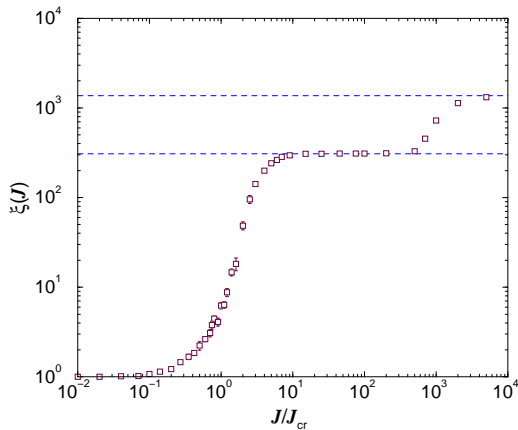
FIG. 5: Inverse participation ratio ξ as a function of the coupling parameter J/J_{cr} for the AA model of Eq. (25), for a chain of size $L = 12$. The IPR is averaged over all eigenfunctions in the central band of the spectrum and over 10 random realizations. The dashed horizontal lines correspond to $N_b/3$ and to $N/3$ where $N = 2^L$ is the dimension of the Hilbert space.

uniformly distributed in the interval $[-1, 1]$. This model is known as the NN model from its nearest neighbor character.

As in the two-dimensional model (18), for the unperturbed ($J = 0$) case the spectrum possesses a band structure. Each band is characterized by a constant number n of qubits in the state $|0\rangle$ and $L - n$ qubits in the state $|1\rangle$. When L is even, a central band (around zero) exists. It consist of the many-qubit states with $L/2$ spins "up" and $L/2$ spins "down". The number of these states is given by

$$N_b = \frac{L!}{(L/2)! \, (L/2)!} \; . \tag{24}$$

In what follows we will only consider the energy levels and energy eigenstates corresponding to the central band of the spectrum.

As discussed above, when $J > 0$ the potential term V mixes the states inside each band and among different bands: In the basis of H_0, V_{diag} is diagonal. Instead, V_{band} couples states which are either in the same band or in next to nearest bands. V_{off} couples states which are in nearest neighbor bands. The mixing of energy bands triggers the transition to chaos. For a relatively weak interaction the eigenstates (in the basis of H_0) are localized, while for stronger interaction the number of components significantly different from zero increases. The transition from strongly localized to extended states occurs very fast with the increase of the interaction and sets in when the strength of the typical interaction is of the order of the mean level spacing between directly coupled many-body states [14]. In [13] the critical value for the delocalization border was found to be $J_{\text{cr}} \approx 4a^2/\Omega$.

However, as it was shown in [13], the NN model is pe-

culiar in the following sense: The delocalization border does not coincide with the chaos border. Increasing the strength of the interaction J, the system goes from a regular regime to a *weak chaos* regime where the eigenfunctions are delocalized but the level statistics is not yet described by Random Matrix Theory. If the interaction is further increased the bands overlap and the system enters a regime of *strong chaos*. This peculiarity is removed if the range of the interaction is larger than nearest neighbor.

Here we will consider a range of the interaction l_c from 1 (for the NN model) up to $L - 1$. The interaction term V keeps the same structure as in Eq. (22) but the different terms are now

$$V_{\text{diag}} = -\frac{1}{2} \sum_{j=1}^{L-1} \sum_{k=j+1}^{j+l_c \leq L} J_{jk} b_j b_k \sigma_j^z \sigma_k^z,$$

$$V_{\text{band}} = -\frac{1}{2} \sum_{j=1}^{L-1} \sum_{k=j+1}^{j+l_c \leq L} J_{jk} a_j a_k \sigma_j^y \sigma_k^y, \tag{25}$$

$$V_{\text{off}} = \frac{1}{2} \sum_{j=1}^{L-1} \sum_{k=j+1}^{j+l_c \leq L} J_{jk} \left(a_j b_k \sigma_j^y \sigma_k^z + a_k b_j \sigma_j^z \sigma_k^y \right) \; .$$

For $l_c = L - 1$ this model is known as the AA (All to All) model as in this case all qubits are allowed to interact with each others. In contrast with the NN model ($l_c = 1$), if $l_c > 1$ the chaos border occurs at the same value $J_{\text{cr}} \approx 4a^2/\Omega$ as the delocalization border [13].

2. The onset of quantum chaos.

In Fig. 4 the nearest level spacing distribution is shown for the AA model for a chain of 12 qubits. The $P(s)$ distribution was obtained from the energy levels contained in the central band and averaged over 10 different random realizations. In panel a, the case of weak interaction ($J/J_{cr} = 0.35$) is shown. It is in good agreement with the Poisson distribution (solid line), as expected in the integrable regime. In contrast, panel b shows the situation corresponding to strong coupling ($J/J_{cr} = 15$) in which the $P(s)$ distribution follows the Wigner surmise expected for a chaotic system with GOE statistics. In panel b, the level repulsion effect is evident. Thus, when the interaction strength $J > J_{cr}$, the spectral level statistics changes from Poisson to GOE showing that a transition to quantum chaos is happening.

Simultaneously, a localization-delocalization transition occurs for the eigenstates in the central band. This transition takes place for any value of l_c. However, for the NN model, the IPR does saturate at a value which is lower than $N_b/3$ corresponding to the case of Gaussian fluctuations. In Fig. 5, the IPR is shown for the AA model for a chain composed of 12 qubits. The IPR (squares) is averaged over all the eigenstates in the central band and over 30 different random realizations. For weak interactions, the eigenstates are effectively localized ($\xi \approx 1$).
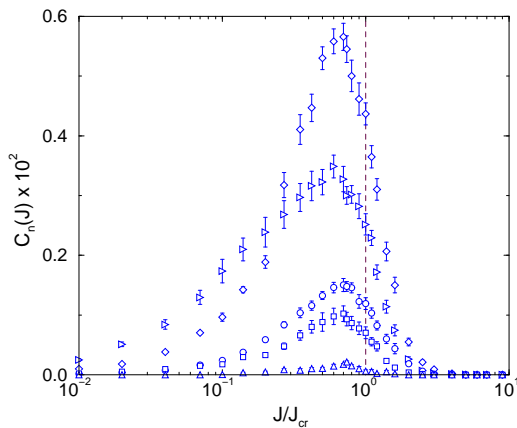
FIG. 6: Concurrence as a function of the coupling parameter J/J_{cr} for the model of Eq. (25) with interaction range $l_c = 5$ for a chain of 10 qubits. For each eigenfunction C_n was obtained as the average concurrence between all possible pairs of qubits separated by a distance n: $n = 1$ for nearest neighbors pairs (diamonds), $n = 2$ for next to nearest neighbors pairs (right-triangles), $n = 3$ (circles), $n = 4$ (squares) and $n = 5$ (up-triangles). The plotted values correspond to C_n averaged over all the eigenstates in the center of the spectrum and over 30 random realizations.

FIG. 7: Mean concurrence C_3 between qubits at a distance $n = 3$, averaged over all the eigenfunctions in the central band of the spectrum and over 30 random realizations. The mean concurrence is plotted as a function of the coupling parameter J/J_{cr} for the model of Eq. (25) in a chain of 10 qubits. We compare C_3 for different range of the interaction: the NN model corresponding to $l_c = 1$ (diamonds), $l_c = 2$ (triangles), and $l_c = 3$ (circles).

The IPR increases monotonously with the interaction until it reaches the value $N_b/3 = 308$ (lower dashed line). A complete mixing of different bands occurs for much stronger interactions ($J/J_{cr} \approx 1000$). This is seen in Fig. 5, where ξ increases again and reaches a value corresponding $N/3$, namely to one third of the dimension of the whole Hilbert space, as expected from RMT.

The model of Eq. (25) shows a clear transition to quantum chaos in which both energy levels and eigenstates change their character. Now we turn our attention to the behavior of quantum entanglement. We start by analyzing the behavior of the concurrence across the quantum transition to chaos.

3. The concurrence: Sharing of entanglement.

We have calculated the mean concurrence averaged over all the eigenstates in the central band as a function of the strength J of the interaction. In Fig. 6 the mean concurrence is shown for the model of Eq. (25) for a chain of $L = 10$ qubits, with an interaction that couples $L/2$ neighbor qubits, i.e., $l_c = 5$. The diamond symbols correspond to the mean concurrence C_1 between nearest neighbor qubits . As it was discussed in section III C, we observe that C_1 is close to zero in both extremes of chaos and of integrability. Moreover, similarly to what we have observed for the two-dimensional model (18), in between the integrable and the chaotic extremes the concurrence increases and its maximum value is close to the critical value for the chaos border. Despite the fact that we have
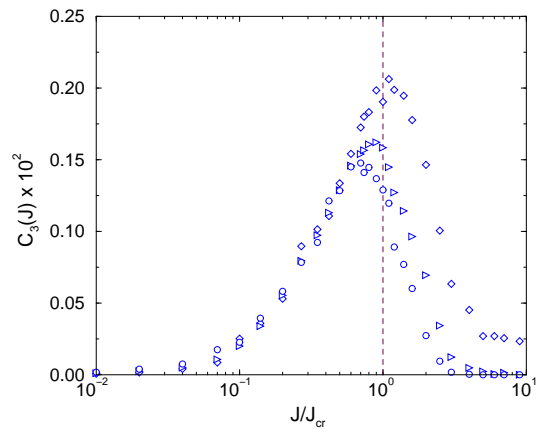
observed this behavior of concurrence for just two different models we conjecture that it is generic for transitions to chaos. We note that a similar behavior for the concurrence has also been observed for quantum phase transitions occurring in integrable models (see, e.g., [21]). In Fig. 6 the mean concurrence averaged over all qubits at further distances, C_2 (right-triangles), C_3 (circles), C_4 (squares) and C_5 (up-triangles) are also shown. The behavior of C_1 and C_2 is similar to that observed for the two-dimensional model. We see that the concurrence C_n decreases with the distance n, except for weak interactions for which $C_2 > C_1$. This latter is a peculiarity of this model. It is interesting to notice that the coupling strength $J_{max}(n)$ at which the concurrence C_n takes its maximum value does not change significantly with n.

Let us now consider the following question: for a given distance n, how does C_n varies if the range of the interaction increases? In Fig. 7 the mean concurrence C_3 is plotted for different ranges l_c of the interaction: $l_c = 1$ (diamonds), $l_c = 2$ (triangles) and $l_c = 3$ (circles). To this purpose, we computed C_3 for all the eigenfunctions in the central band of the spectrum of a chain of size $L = 10$ and averaged over 30 different random realizations. From Fig. 7 we observe that as the range of the interaction increases the mean concurrence C_3 decreases. The same conclusions were also obtained for the behavior C_n with $n \neq 3$ (data not shown). This fact can be understood from the pairwise character of the concurrence. Since the amount of entanglement between one definite qubit and the rest of the system is bounded, this finite amount of entanglement has to be shared among all possible partners. When the range of the interaction is enlarged, it becomes easier for each qubit to become
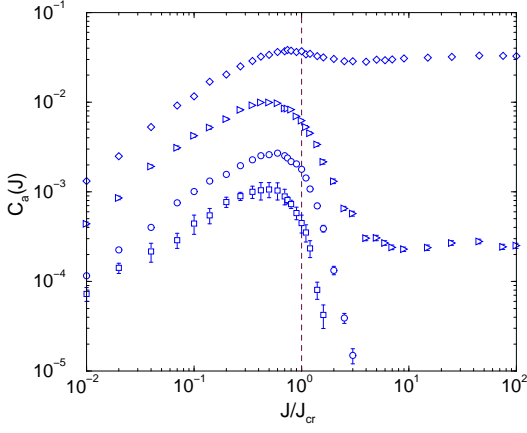
FIG. 8: Mean concurrence averaged over all possible pairs of qubits for all the eigenstates in the central band of the spectrum and over 30 random realizations for the AA model of Eq. (25) ($l_c = L - 1$) as a function of the coupling parameter J/J_{cr} and for different sizes of the chain of qubits: $L = 6$ (diamonds), $L = 8$ (triangles), $L = 10$ (circles), $L = 12$ (squares).
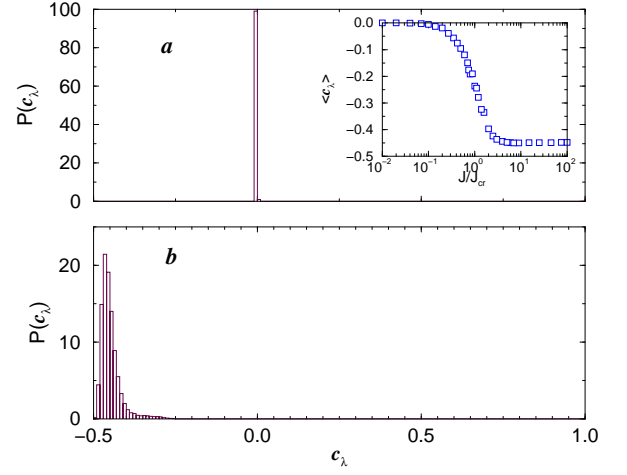

FIG. 9: Normalized distribution $P(c_\lambda)$ of the quantity $c_\lambda = \lambda_1 - \lambda_2 - \lambda_3 - \lambda_4$ of Eq. (5) for the AA model Eq. (25) with $L = 12$ and coupling: a) $J/J_{cr} = 0.01$ and b) $J/J_{cr} = 100.0$. In the inset the behavior of the first moment of the distribution $< c_\lambda >$ is shown as a function of the coupling parameter J/J_{cr}.

entangled with more qubits in the chain. As a result the pairwise entanglement between one single qubit and the rest of the chain is shared among more partners. Therefore, the average entanglement shared between two qubits decreases. This argument is valid if a change in the range of the interaction does not significantly change the total amount of bipartite entanglement that is shared between a single qubit and the rest of the chain.

Finally, we have studied the behavior of the concurrence as a function of the size of the system. In Fig. 8 the mean concurrence C_a obtained from all possible pairs of qubits is shown for the AA model for different sizes of the chain: $L = 6$ (diamonds), $L = 8$ (triangles), $L = 10$ (circles), $L = 12$ (squares). In this case, instead of measuring the concurrence C_n for some value of n, we have measured the concurrence C_a as the mean concurrence between all possible pairs of qubits in the chain. This is because, for the AA model, the concept of distance turns out to be meaningless, since the strength of the interaction between two qubits does not depend on their distance. The behavior of C_a as a function of the size of the system can be well understood in terms of the same argument used to explain Fig. 7. When the system size is increased, the number of possible partners with which a given qubit can be entangled also increases. Therefore, the pairwise entanglement decreases, in agreement with the data of Fig. 8. We note that, for small system sizes ($L = 6, 8$), the concurrence C_a does not go to zero at the chaotic side of the transition. This finite-size effect disappears already for $L = 10, 12$.

It is interesting to study the different character of mixed pairwise entanglement in the integrable and chaotic sides of the transition. In Sec. III C, we gave simple arguments that explain the different structure of the

reduced density matrix $\tilde\rho$ for a mixed bipartite state in the regimes of integrability and chaos. In the integrable region, due to the localized nature of the eigenstates, $\tilde\rho$ is essentially diagonal with only one matrix element significantly different from zero. On the other hand, in the chaotic region, $\tilde\rho$ is almost diagonal with matrix elements of comparable magnitude along the diagonal. Both cases give a very small (or zero) concurrence. However, while in the integrable case this is due to the fact that the two-qubit subsystem under investigation is essentially in a separable pure state, in the chaotic case the pairwise entanglement is zero due to the random structure of the eigenfunctions of the whole L-spin system. As a consequence, the two-qubit reduced density matrix is essentially diagonal. Therefore, in the chaotic regime, the interaction with the rest of the system mimics a decoherence process for the two-qubit subsystem.

The different origin of the very small value of concurrence is illustrated by the distribution of the c_λ's (we remind the reader that the concurrence is defined as the maximum between c_λ and 0, see Eq. (5)). In Fig. 9, the probability distribution $P(c_\lambda)$ is shown in: a) the integrable regime and b) the chaotic regime, for the AA model and a chain of size $L = 12$. Clearly, in both cases the probability to find $c_\lambda > 0$ is very small. Therefore, the concurrence is very small in both cases. However, the distributions $P(c_\lambda)$ are quite different. We note that numerical results about the distribution $P(c_\lambda)$ in a different model of quantum chaos where presented in [34]. In the Inset of Fig. 9, one can see that the first moment of $P(c_\lambda)$ changes across the chaos border. It is an interesting open problem to obtain an analytical form of $P(c_\lambda)$ for integrable and chaotic situations. The possibility to
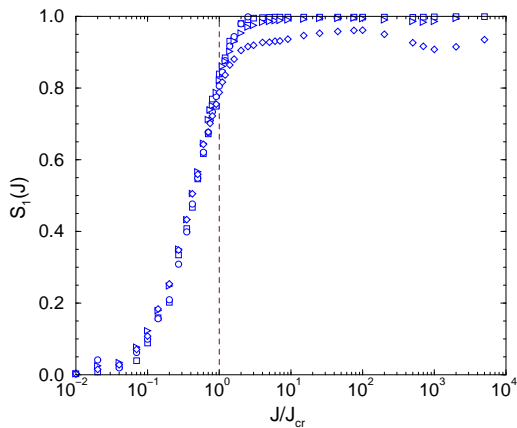
FIG. 10: Von Neumann entropy S_1 between one qubit and the rest of the system; S_1 is averaged over all qubits and over all eigenstates in the central band of the spectrum and over 30 random realizations for the AA model of Eq. (25) as a function of the coupling parameter J/J_{cr} and for different sizes of the chain of qubits: $L = 6$ (diamonds), $L = 8$ (triangles), $L = 10$ (circles), $L = 12$ (squares).
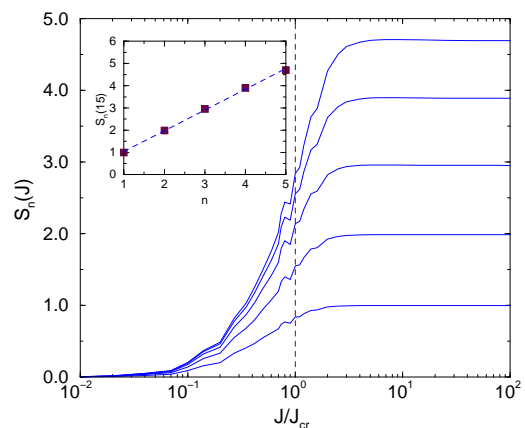

FIG. 11: Von Neumann entropy S_n between left and right blocks of sizes n and $L - n$ qubits, respectively, averaged over all eigenfunctions in the central band of the spectrum and over 10 random realizations. The data correspond to the AA model of Eq. (25) for a chain of size $L = 12$. From bottom to top, the different curves are from $n = 1$ to $n = 5$. In the inset $S_n(J/J_{cr} = 15)$ is plotted as a function of n. The dashed line corresponds to a linear fit with a slope of 0.93 ± 0.02.

use this distribution to mark the transition to chaos also deserves more investigation.

4. The Von Neumann entropy.

We now turn our attention to the behavior of bipartite entanglement measured in terms of the Von Neumann entropy. First we consider the mean Von Neumann entropy S_1 of each qubit with the rest of the qubits in the chain. For this purpose, we divide the system in two parties: one consists of just one qubit and the other contains the remaining $L - 1$ qubits. Then, following Eq. (1), we compute S_1 from the 2×2 reduced density matrix of the one qubit subsystem. In Fig. 10 the behavior of S_1 across the transition to chaos is shown for the AA model and for different sizes of the system, from $L = 6$ to $L = 12$. We find that the bipartite entanglement S_1 shows the same behavior independently of the size of the system. The state of the system changes from separable to maximally entangled as the transition to chaos occurs. In all cases, the entropy saturates to its maximum value $S_1 = 1$, up to corrections of order $1/2^L$ [54]. As discussed in Sec. II, these results show that there exists a global entanglement of each single qubit with the rest of the system and that this entanglement increases with the interaction. The maximum value of bipartite entanglement is obtained when quantum chaos has set in. The same conclusions are seen to hold for a genuine multipartite entanglement measure introduced in [44] (data not shown).

We have obtained similar results for the bipartite entanglement when the two blocks in which the system is partitioned have different lengths. As an example we

show in Fig. 11 the Von Neumann entropy S_n between a block of size n and the rest of the system (of size $L - n$) from $n = 1$ (bottom) to $n = 5$ (top) for the AA model and a chain of size $L = 12$. Similarly to the S_1 case, S_n increases when the transition to chaos occurs and saturates to $S_n \approx n$ for large interaction strength. Hence, the state of the system becomes maximally entangled when chaos sets in. This is a direct consequence of the existence of multipartite entanglement. Moreover, in the inset of Fig. 11, we have plotted the saturation value of S_n for $J/J_{cr} = 15$ as a function of the size of subsystems n. This shows that in the chaotic regime the bipartite entanglement scales linearly with the size of the smallest of the two blocks in which the global system has been partitioned: $S_n \propto n$.

It is interesting to study the Von Neumann entropy as a function of the system size L, when the two blocks in which the system is partitioned have a size $\propto L$. We have computed the bipartite entanglement $S_{L/2}$ corresponding to the case in which the system is partitioned in two halves. A value of $S_{L/2} > 0$ for any L is indicative of the existence of multipartite entanglement. The obtained behavior of $S_{L/2}$ as a function of the strength of the interaction is shown in Fig. 12, for different system sizes. The behavior of $S_{L/2}$ is similar to that shown by S_1. It takes very small values in the integrable regime and then increases with the interaction up to a value for which it saturates. The saturation value is $\approx L/2$ (up to corrections of $\mathcal{O}(1)$ [54]). In the inset of Fig. 12, we plot the value of $S_{L/2}$ for $J/J_{cr} = 15$ (i.e., in the chaotic regime in which the eigenstates in the central band are effectively mixed) as a function of the size L of the system. It is interesting to note that the Von Neumann
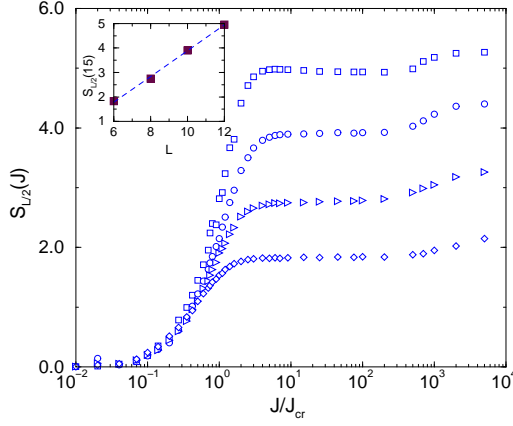
FIG. 12: Von Neumann entropy $S_{L/2}$ as a function of the strength of the interaction J/J_{cr}, averaged over all eigenfunctions in the central band of the spectrum and over 10 random realizations. The data correspond to the AA model of Eq. (25) for a chain of sizes $L = 6$ (diamonds), $L = 8$ (triangles), $L = 10$ (circles), $L = 12$ (squares). In the inset $S_{L/2}(J/J_{cr} = 15)$ is plotted as a function of L. The dashed line corresponds to a linear fit with a slope of 0.52 ± 0.02.

entropy does feel the mixing of different spectral bands occurring for a very strong interaction ($J/J_{cr} \sim 1000$). The inter-band mixing (compare with Fig. 5 for $L = 10$) produces a increase in the Von Neumann entropy which nevertheless is small compared to that observed for the onset of chaos. The same was also observed for the multipartite measure of [44]. This is in contrast with the pairwise measures such as the concurrence, for which we did not observed any change.

In addition, for any given value of J when chaos has set in, the bipartite entanglement scales linearly with the size of the system. It is interesting to comment this result from the viewpoint of computational complexity. It was shown in [56] that large entanglement of the quantum computer hardware is a necessary condition for exponential speedup (with respect to classical computation) in quantum computation operating on pure states. To be more precise, a necessary condition for an exponential speedup is that the amount of entanglement increases greater than logarithmically with the size L of the computation. This condition is fulfilled in the chaotic regime where $S_{L/2} \propto (L/2)$. We remark that, differently from problems like exact cover [57], this is not limited to the transition region but extends to the whole chaotic regime.

5. *Weak and hard chaos*

In this section, we discuss the behavior of quantum entanglement in situations of weak and of hard chaos. As it was discussed, the NN model of Eq. (22), while similar in character to the model of Eq. (25) with $l_c > 1$, shows a quite unexpected peculiarity: The chaos border does not
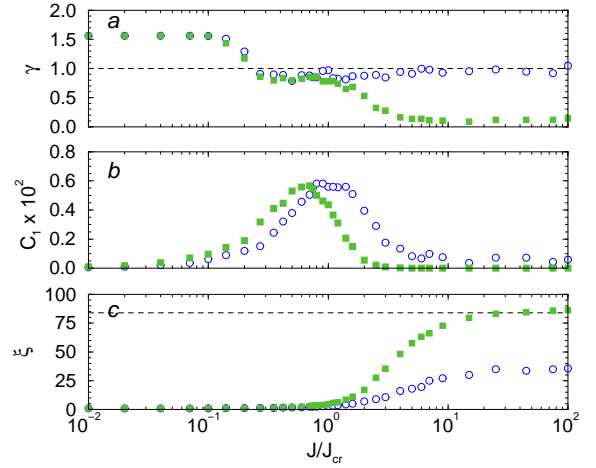

FIG. 13: Comparison between the NN model Eq. (22) (circles) and the model of Eq. (25) with $l_c = L/2$ (squares), for a chain of qubits of length $L = 10$. From top to bottom, the three panels show, as a function of the coupling parameter J/J_{cr}: the behavior of the spectral statistics parameter γ (top panel); the mean concurrence C_1 between nearest neighbor pairs of qubits (middle panel); the inverse participation ratio ξ (bottom panel). All quantities were calculated in the central band of the spectrum and averaged over 30 random realizations.

coincide with the delocalization border. Thus, when the strength of the interaction is increased, the NN model experiences a transition from integrability to a situation of weak chaos in which the eigenfunctions are delocalized while the level statistics is yet of Poissonian nature. This results from the fact that the NN Hamiltonian can be approximately mapped into a model of L free fermions as discussed in [55]. However, this non generic situation is removed if longer ranges of the interaction are considered. This gives us the possibility to compare the behavior of entanglement in situations of weak and hard chaos.

We have calculated the nearest neighbor concurrence C_1 for the NN model and for a long range interaction model with $l_c = L/2$. In Fig. 13 we present our results. In panels (a) and (c) the γ parameter and the IPR ξ are shown, respectively. We can clearly see the peculiar behavior of the NN model. For both NN (open circles) and $l_c = L/2$ (solid squares) models the IPR behaves in a similar way. For the NN model the IPR signals a clear transition from localized to delocalized eigenstates, even thought it does not saturates at the value corresponding to Gaussian fluctuations. In particular, the delocalization border of both models coincide. Nevertheless, the γ parameter shows a very different behavior. For interaction strengths $0.2 \leq J/J_{cr} \leq 1$ the level statistics parameter γ for both models takes the value $\gamma \approx 1$. This corresponds to the integrable case in which the nearest neighbor spacing distribution is Poissonian. However, for the NN model, γ remains Poissonian for larger values of the interaction up to $J/J_{cr} \approx 100$. This is the situa-

tion that has been termed as weak chaos. In contrast, for the $l_c = L/2$ model the level statistics changes from Poissonian ($\gamma = 1$), to GOE ($\gamma = 0$), around $J/J_{cr} = 1$. Thus, for the $l_c = L/2$ model the chaos border coincides with the delocalization border as it is commonly found in many-particle systems with two-body interaction.

In panel (b) the corresponding results for the concurrence C_1 are shown. We observe again the difference in C_1 due to the range of the interaction, as discussed in the previous subsection. Despite this difference, C_1 shows a similar behavior for both models: It is small at both sides of the transition and increases in between, having its maximum value close to $J/J_{cr} = 1$. This numerical results suggest that the behavior of the pairwise entanglement is more sensitive to the mixing of the eigenstates than to the onset of quantum chaos.

V. FINAL REMARKS

We have studied the bipartite and pairwise entanglement in one- and two-dimensional spin lattice models that experience a transition to quantum chaos.

To study the presence of multipartite entanglement, we have analyzed the behavior of the averaged Von Neumann entropy for subsystems of different sizes. In particular, we have shown that, for a partition of the system into two equal-size subsystems, this quantity grows linearly with the system size in the chaotic regime. This shows that the classical simulation method discussed in [56] cannot be used to efficiently simulate the quantum

chaos regime on a classical computer.

For the case of pairwise entanglement, we have studied the dependence of the concurrence on the distance between the partners, the range of the interaction and the size of the system. Our results show that, as the range of the interaction and/or the size of the system increases, the average entanglement between two qubits decreases, since the entanglement is shared among more partners.

We have also discussed the different character that the pairwise entanglement has at the integrable and the chaotic side of the transition in terms of a suitable distribution of the eigenvalues of the two-spin reduced density matrix. The use of the moments of this distribution to mark the transition to quantum chaos remains and interesting open question.

Finally, we have found that the concurrence exhibits its maximum close to the value of the interaction (delocalization border) for which mixing of the noninteracting eigenfunctions takes place. This value is not necessarily related to the onset of quantum chaos.

[1] M.A. Nielsen and I.L. Chuang, *Quantum Computation and Quantum Information* (Cambridge University Press, Cambridge, 2000).

[2] G. Benenti, G. Casati, and G. Strini, *Principles of Quantum Computation and Information*, Vol. I: *Basic concepts* (World Scientific, Singapore, 2004).

[3] R. Jozsa and N. Linden, Proc. R. Soc. Lond. A **459**, 2011 (2003).

[4] C. Miquel, J.P. Paz, and R. Perazzo, Phys. Rev. A **54**, 2605 (1996).

[5] C. Miquel, J.P. Paz, and W.H. Zurek, Phys. Rev. Lett. **78**, 3971 (1997).

[6] P.H. Song and D.L. Shepelyansky, Phys. Rev. Lett. **86**, 2162 (2001).

[7] G.G. Carlo, G. Benenti, and G. Casati, Phys. Rev. Lett. Phys. Rev. Lett. **91**, 257903 (2003); G.G. Carlo, G. Benenti, G. Casati, and C. Mejía-Monasterio, Phys. Rev. A **69**, 062317 (2004).

[8] D. Rossini, G. Benenti, and G. Casati, Phys. Rev. A **69**, 052317 (2004).

[9] P. Facchi, S. Montangero, R. Fazio, and S. Pascazio, quant-ph/0407098.

[10] B. Georgeot and D.L. Shepelyansky, Phys. Rev. E **62**, 3504 (2000); *ibid.* **62**, 6366 (2000).

[11] V.V. Flambaum, Aust. J. Phys. **53**, 489 (2000).

[12] G. Benenti, G. Casati, and D.L. Shepelyansky, Eur. Phys. J. D **17**, 265 (2001).

[13] G.P. Berman, F. Borgonovi, F.M. Izrailev, and V.I. Tsifrinovich, Phys. Rev. E **64**, 056226 (2001); *ibid.* **65**, 015204(R) (2002).

[14] V. Zelevinsky, B.A. Brown, N. Frazier and M. Horoi Phys. Rep. **276**, 85 (1996); V.K.B. Kota, Phys. Rep. **347**, 223 (2001); L. Benet and H.A. Weidenmüller J. Phys. A: Math. Gen. **36**, 3569 (2003)

[15] G. Montambaux, D. Poilblanc, J. Bellissard and C. Sire, Phys. Rev. Lett., **70**, 497 (1993); D. Poilblanc, T. Ziman, J. Bellissard, F. Mila and G. Montambaux, Europhys. Lett., **22**, 537 (1993); T.C. Hsu and J.C. Anglès d'Auriac, Phys. Rev. B., **47**, 14291 (1993); Y. Avishai, J. Richert and R. Berkovits, Phys. Rev. B., **66**, 052416 (2002); J.Ch. Anglès d'Auriac and J.-M. Maillard, Physica A, **321**, 325 (2003);

[16] F.M. Izrailev, *in* [49], p. 371, and references therein.

[17] P.A. Lee and T.V. Ramakrishnan, Rev. Mod. Phys. **57**, 287 (1985); U. Sivan and Y. Imry, Phys. Rev. B **35**, 6074 (1987); B.I. Shklovskii, B. Shapiro, B.R. Sears, P. Lambrianides and H.B. Shore, Phys. Rev. B **47**, 11487 (1993); I. K. Zharekeshev and B. Kramer,Phys. Rev. B **51**, R17239 (1995).

[18] S. Sachdev, *Quantum Phase Transitions* (Cambridge

University Press, Cambridge, 1999).

[19] T.J. Osborne and M.A. Nielsen, Quantum Information Processing **1**, 45 (2002).

[20] A. Volya and V. Zelevinsky, Phys.Lett. **B574**, 27 (2003).

[21] A. Osterloh, L. Amico, G. Falci, and R. Fazio, Nature **416**, 609 (2002); L. Amico, A. Osterloh, F. Plastina, R. Fazio, and G.M. Palma, Phys. Rev. A **69**, 022304 (2004).

[22] T.J. Osborne and M.A. Nielsen, Phys. Rev. A **66**, 032110 (2002).

[23] I. Bose and E. Chattopadhyay, Phys. Rev. A **66**, 062320 (2002).

[24] G. Vidal, J.I. Latorre, E. Rico, and A. Kitaev, Phys. Rev. Lett. **90**, 227902 (2003).

[25] S.J. Gu, H.Q. Lin, and Y.Q. Li, Phys. Rev. A **68**, 042330 (2003).

[26] U. Glaser, H. Büttner, and H. Fehske, Phys. Rev. A **68**, 032318 (2003).

[27] V.E. Korepin, Phys. Rev. Lett. **92**, 096402 (2004).

[28] J. Vidal, G. Palacios, and R. Mosseri, Phys. Rev. A **69**, 022107 (2004); J. Vidal, R. Mosseri, and J. Dukelsky *ibid.* 69, 054101 (2004).

[29] F. Verstraete, M. Popp, and J.I. Cirac, Phys. Rev. Lett. **92**, 027901 (2004).

[30] S. Montangero, G. Benenti, and R. Fazio, Phys. Rev. Lett. **91**, 187901 (2003).

[31] L.F. Santos, G. Rigolin, and C.O.Escobar, Phys. Rev. A **69**, 042304 (2004).

[32] N. Lambert, C. Emary, and T. Brandes, Phys. Rev. Lett. **92**, 073602 (2004).

[33] S. Bettelli and D.L. Shepelyansky, Phys. Rev. A **67**, 054303 (2003).

[34] A.J. Scott and C.M. Caves, J. Phys. A **36**, 9553 (2003).

[35] A. Lahiri, quant-ph/0302029.

[36] X. Wang, S. Ghose, B.C. Sanders, and B. Hu, quant-ph/0312047.

[37] W.K. Wootters, Quantum Inf. and Comp. **1**, 27 (2001).

[38] C.H. Bennett, D.P. DiVincenzo, J.A. Smolin, and W.K. Wootters, Phys. Rev. A **54**, 3824 (1996).

[39] W.K. Wootters, Phys. Rev. Lett. **80**, 2245 (1998).

[40] C.H. Bennett, G. Brassard, S. Popescu, B. Schumacher, J.A. Smolin, and W.K. Wootters, Phys. Rev. Lett. **76**, 722 (1996).

[41] K. Zyczkowski, P. Horodecki, A. Sanpera, and M. Lewenstein, Phys. Rev. A **58**, 883 (1998); G. Vidal and R.F. Werner, *ibid.* **65**, 032314 (2002).

[42] V. Vedral, M.B. Plenio, K. Jacobs, and P.L. Knight, Phys. Rev. A **56**, 4452 (1997).

[43] D. Bruß, J. Math. Phys. **43**, 4237 (2002).

[44] D.A. Meyer and N.R. Wallach, J. Math. Phys. **43**, 4273 (2002).

[45] G.K. Brennen, Quantum Inf. and Comp. **3**, 619 (2003); see also A.J. Scott, Phys. Rev. A, **69**, 052330 (2004).

[46] E.P. Wigner, Ann. Phys. (N.Y.) **53**, 36 (1951); *ibid.* **62**, 548 (1955); *ibid.* **67**, 325 (1958); F.J. Dyson, J. Math. Phys. **3**, 140 (1962); M.L. Mehta, *Random Matrices and the Statistical Theory of Energy Levels* (Academic Press, New York, 1967);

[47] T.A. Brody, J. Flores, J.B. French, P.A. Mello, A. Pandey, and S.S.M. Wong, Rev. Mod. Phys. 53, 385 (1981).

[48] T. Guhr, A. Müller-Groeling, and H.A. Weidenmüller, Phys. Rep. **299**, 189 (1998).

[49] *New Directions in Quantum Chaos*, Proceedings of the International School of Physics "Enrico Fermi", Course CXLIII, Varena (1999), eds. G. Casati, I. Guarneri, and U. Smilansky (IOS Press, Amsterdam, 2000).

[50] F. Haake, *Quantum Signatures of Chaos* (2nd. Ed.), (Springer-Verlag, Berlin, 2000).

[51] O. Bohigas, M.-J. Giannoni, and C. Schmit, Phys. Rev. Lett. **52**, 1 (1984).

[52] G. Casati, F. Valz-Gris, and I. Guarneri, Lett. Nuovo Cimento **28**, 279 (1980).

[53] L. Benet, T.H. Seligman, and H.A. Weidenmüller, Phys. Rev. Lett. **71**, 529 (1993).

[54] D.N. Page, Phys. Rev. Lett. **71**, 1291 (1993); S.K. Foong, S. Kanno *ibid.* **72**, 1148 (1993); S. Sen *ibid.* **77**, 1 (1996).

[55] E. Lieb, T. Schultz, and D. Mattis, Ann. Phys. (N.Y.) **16**, 407 (1961); A.P. Young and H. Rieger, Phys. Rev. B **53**, 8486 (1996).

[56] G. Vidal, Phys. Rev. Lett. **91**, 147902 (2003).

[57] R. Orús and J.I. Latorre, Phys. Rev. A **69**, 052308 (2004).